Control of a two-wheel robotic vehicle for personal transportation

H. W. Kim and S. Jung

Robotica / *FirstView* Article / September 2014, pp 1 - 23
DOI: 10.1017/S0263574714002173, Published online: 10 September 2014

Robotica: page 1 of 23. © Cambridge University Press 2014
doi:10.1017/S0263574714002173

Control of a two-wheel robotic vehicle for personal transportation

H. W. Kim and S. Jung*

Intelligent Systems and Emotional Engineering (ISEE) Laboratory, Department of Mechatronics Engineering, Chungnam National University, Daejeon, Korea

(Accepted July 21, 2014)

SUMMARY
Recently, small-sized compact electric vehicles have been in demand for short-distance travel in urban areas, although battery charging in electric vehicles present in the market is still problematic. Borrowing from the concept of a mobile inverted pendulum system, in this paper, a two-wheel robotic vehicle system is implemented and controlled as the future personal transportation device called the TransBOT. The TransBOT has two driving modes: a regular vehicle mode, where stable contact on the ground is maintained by two wheels and two casters, and the balancing mode, which maintains the stable posture with two wheels on the ground. The two-wheel balancing mechanism can be used as a transportation vehicle in narrow and busy urban areas. Gain scheduling control methods based on linear controllers are used for different drivers. In addition, desired balancing angles are specified for the different sizes of drivers in order to have a stable balancing control performance. These desired balancing angle values have been found by empirical studies. Experimental studies with drivers of different weights, as well as indoor and outdoor driving tasks, were conducted to ensure the feasibility of TransBOT.

KEYWORDS: Two-wheel robot; Personal vehicle; Sensor fusion; Balancing control.

1. Introduction

Nowadays, car manufacturers are producing a low percentage of cars with combustion engines. Instead, they are using electric motors for various reasons, including air pollution and gas exhaustion. Hybrid vehicles are in the middle of a combustion engine vehicle and an electric vehicle. Various governments are aiding in transition to hybrid vehicles and providing financial support for its development.

Furthermore, consumers find small-sized compact electric vehicles attractive, creating demand for such vehicles. Some of the small-compact electric vehicles are already in the market, although various practical problems, such as regulations that allow electrical vehicles to run on the road and the construction of charging stations, are yet to be solved. In spite of these difficulties, there is no doubt that in the future electric vehicles will be used for transportation.

In the framework of robotic vehicles, mobile robots are defined as electric vehicles if they carry people as passengers. Mobile robots have the potential to carry objects in addition to passengers; in fact, they have been used for transportation for a long time, although their applications were previously focused on unmanned autonomous navigation and surveillance. Most of the mobile robot research has been focused on autonomous navigation for various purposes such as delivering objects, search and rescue missions, exploring extreme weather locations, and so on.

Electric vehicles have been around for a long time, the most notable being the golf cart and small wheelchair vehicles. Now, mobile robot technology and electric automobile technology have merged, creating a new area for robotic vehicles.

The most popular personal robotic vehicle is the Segway, which is driven on two wheels.[1] Many research institutes have elaborated on the balancing control technology of a two-wheel platform

* Corresponding author. E-mail: jungs@cnu.ac.kr

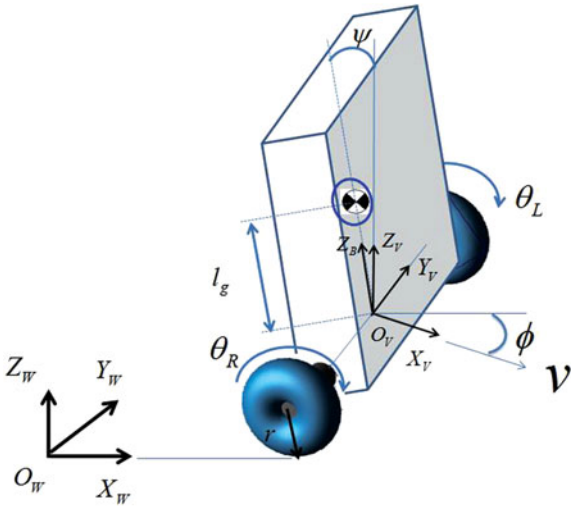

Fig. 1. (Colour online) Configuration of TransBOT.

in different ways. A two-wheel inverted pendulum has been implemented[2,3] and controlled by a neural network[4] and fuzzy logic.[5] A two-wheel scooter was developed with a similar structure as that of the Segway to carry human passengers.[6,7] Two-wheel mobile manipulators were developed as extensions; these make use of an arm[8] and humanoid arms.[9,10] Other two-wheel-based mobile robots are developed for entertainment purposes.[11,12] The interaction control of two-wheel mobile robots with the environment has been considered.[13–15] Sensor fusion methods for two-wheel mobile robots have been also investigated.[16,17] A two-wheel robot uses a camera to detect driving lanes, and maneuvering within a driving lane has been demonstrated.[18] A vertical drive mechanism for a two-wheel mobile robot has been also developed,[19] and stable two-wheel mobile robots have been demonstrated. More challengingly, the control of single-wheel robots has been also presented.[20,21]

Although two-wheel robotic vehicles are compact in size and efficient in driving, the driver has to stand for the entire time while traveling to destination. This is less appealing to potential buyers, because passengers are limited by age and gender. Thus, a more comfortable personal vehicle for urban areas is desired not only for transportation in order to commute but also as a touring vehicle. Autonomous road vehicles for passengers have been presented.[22] A group of engineers demonstrated a mini car system that functioned as an urban transportation system and operated on a road network,[23,24] in addition to the demonstration of a GPS-based control of a car-like vehicle.[25] Recently, Segway has developed personal urban mobility and accessibility (PUMA) as a transportation vehicle for people of urban settings so that two drivers can drive it sitting for traveling short distances.[1] A two-wheel chair robot has also been developed.[26]

In this paper, the feasibility of a robot that carries people as passengers for urban transportation was studied as an extension of our previous paper.[27] A new car-like robotic vehicle, TransBOT, was designed, implemented, and controlled based on a two-wheel mechanism. The TransBOT is a robotic vehicle that performs the functions of vehicles such as carrying people or objects.

The TransBOT has two driving modes: the four-wheel contact mode, which is stabilized by casters, and the two-wheel balancing mode, which mimics the concept of inverted pendulum when the front casters are lifted. Experimental studies were conducted to test the feasibility of using the balancing mechanism for transportation. The balancing mechanism was tested for different body types and weights of drivers. The balancing mechanism was tested outdoors as well as in the indoor environment.

2. Modeling of TransBOT

2.1. Kinematics

The kinematic configuration of TransBOT is shown in Fig. 1. For the analysis provided in this paper, the important variables for the positioning of the vehicle are the positions x and y, and the two angles

Table I. Definitions of variables of the model.

Variables	Units	Description
m_b	kg	Mass of the body
m_w	kg	Mass of the wheel
l_g	M	Distance from the center of gravity to the center of wheel axis in the z-direction
L	M	Distance between two wheels
r	M	Radius of the wheel
d	M	Distance from the center of gravity to the center of wheel axis in the y-direction
I_{xx}, I_{yy}, I_{zz}	kgm^2	Moment of inertia of body on the ($O_m X_m Y_m Z_m$) axis
I_{COM}	kgm^2	Moment of inertia of body at COM on the ($O_m X_m Y_m Z_m$) axis

ϕ and ψ. Since the TransBOT combines a mobile robot with an inverted pendulum system, variables x, y, and ϕ determine the position of mobile base. The variable ψ is the balancing angle of the inverted pendulum system.

We assumed that the center of the mass (COM) is located along the z-direction from the center of the wheel axis, as shown in Fig. 1. The variables of the model of the TransBOT are listed in Table I.

The kinematic transformation matrix for orientation and translation of vehicle coordinates V ($O_V X_V Y_V Z_V$) with respect to the world coordinates W ($O_W X_W Y_W Z_W$) are given as

$$T_W^V = \begin{bmatrix} \cos\phi & -\sin\phi & 0 & x \\ \sin\phi & \cos\phi & 0 & y \\ 0 & 0 & 1 & r \\ 0 & 0 & 0 & 1 \end{bmatrix}, \tag{1}$$

where x and y are the origins of the coordinate ($O_V X_V Y_V Z_V$) and r is the wheel radius. The position of the vehicle with respect to the coordinate ($O_w X_w Y_w Z_w$) becomes $P_W^V = [x y \phi]^T \in R^{3\times 1}$. Since the vehicle is tilted by the pitch angle ψ on the Y_V-axis, we have the following transformation matrix for the coordinate ($O_V X_V Y_V Z_V$):

$$T_V^B = \begin{bmatrix} \cos\psi & 0 & \sin\psi & 0 \\ 0 & 1 & 0 & 0 \\ -\sin\psi & 0 & \cos\psi & 0 \\ 0 & 0 & 0 & 1 \end{bmatrix}. \tag{2}$$

We assume that the COM of the system is located normally in the center of the wheel axis in the z-direction; the transformation follows:

$$T_B^{\text{COM}} = \begin{bmatrix} 1 & 0 & 0 & 0 \\ 0 & 1 & 0 & 0 \\ 0 & 0 & 1 & l_g \\ 0 & 0 & 0 & 1 \end{bmatrix}, \tag{3}$$

where l_g is the distance from the origin of ($O_B X_B Y_B Z_B$) to the center of gravity position.

Then the coordinates of the center of gravity with respect to global coordinates can be obtained through a series of multiplication with transformation matrices (1), (2), and (3).

$$T_W^V T_V^B T_B^{\text{COM}} = \begin{bmatrix} \cos\phi\cos\psi & -\sin\phi & \cos\iota\sin\psi & x + l_g\cos\phi\sin\psi \\ \sin\phi\cos\psi & \cos\phi & \sin\phi\sin\psi & y + l_g\sin\phi\sin\psi \\ -\sin\psi & 0 & \cos\psi & r + l_g\cos\psi \\ 0 & 0 & 0 & 1 \end{bmatrix}. \tag{4}$$

From (4), the Cartesian position of the COM, $P_W^{\mathrm{COM}} \in R^{3\times 1}$ in the world coordinate $(O_W X_W Y_W Z_W)$ is described as

$$P_W^{\mathrm{COM}} = \begin{bmatrix} x + l_g \cos\phi \sin\psi \\ y + l_g \sin\phi \sin\psi \\ r + l_g \cos\psi \end{bmatrix}. \tag{5}$$

The linear velocity V_W^{COM} can be obtained by differentiating (5) such that $V_W^{\mathrm{COM}} = \dot{P}_W^{\mathrm{COM}}$.

$$V_W^{\mathrm{COM}} = \begin{bmatrix} \dot{x} + l_g(\dot{\psi}\cos\phi\cos\psi - \dot{\phi}\sin\phi\sin\psi) \\ \dot{y} + l_g(\dot{\psi}\sin\phi\cos\psi + \dot{\phi}\cos\phi\sin\psi \\ -l_g\dot{\psi}\sin\psi \end{bmatrix}. \tag{6}$$

The angular velocity Ω at the COM is given by

$$\Omega = \begin{bmatrix} \cos\psi & 0 & \sin\psi \\ 0 & 1 & 0 \\ -\sin\psi & 0 & \cos\psi \end{bmatrix} \begin{bmatrix} 0 \\ 0 \\ \dot{\phi} \end{bmatrix} + \begin{bmatrix} 0 \\ \dot{\psi} \\ 0 \end{bmatrix} = \begin{bmatrix} \dot{\phi}\sin\psi \\ \dot{\psi} \\ \dot{\phi}\cos\psi \end{bmatrix}. \tag{7}$$

2.2. Dynamics

The dynamics of TransBOT is derived by forming the Euler–Lagrangian equation based on the system energy, the kinetic energy, and the potential energy.

The kinetic energy for the body can be derived from the velocity information given in (6) and (7):

$$K_b = \frac{1}{2} m_b V_W^{\mathrm{COM}T} V_W^{\mathrm{COM}} + \frac{1}{2}\Omega^T I_{\mathrm{COM}}\Omega = \frac{1}{2} m_b[\dot{x}^2 + 2\dot{x}l_g(\dot{\psi}c\phi c\psi - \dot{\phi}s\phi s\psi)$$
$$+ \dot{y}^2 + 2\dot{y}l_g(\dot{\psi}s\phi c\psi + \dot{\phi}c\phi s\psi)] + l_g^2(\dot{\psi}^2 + \dot{\phi}^2 s^2\psi) + \frac{1}{2}(I_{xx}\dot{\phi}^2 s^2\psi + I_{yy}\dot{\psi}^2 + I_{zz}\dot{\phi}^2 c^2\psi), \tag{8}$$

where $c\varphi = \cos\varphi$, $s\varphi = \sin\varphi$, $c\psi = \cos\psi$, $s\psi = \sin\psi$, and $s^2\psi = \sin^2\psi$ and $c^2\psi = \cos^2\psi$.

The kinetic energy for the wheel is given as

$$K_w = \frac{1}{2} m_w r^2 \left(\dot{\theta}_R^2 + \dot{\theta}_L^2\right), \tag{9}$$

where m_w is the mass of the wheel and $\dot{\theta}_R^2$ and $\dot{\theta}_L^2$ are respectively the velocity of right and left wheels.

The potential energy is found to be

$$U = m_b g l_g \cos\psi, \tag{10}$$

where g is the gravitational acceleration.

Therefore, the Lagrangian function L_g can be obtained by combining (8), (9), and (10) as

$$L_g = K_b + K_w - U. \tag{11}$$

The dynamic equation of the TransBOT can be obtained from the following equation:

$$\frac{d}{dt}\left(\frac{dL_g}{d\dot{q}}\right) - \frac{dL_g}{dq} = \tau_w, \tag{12}$$

where $q = [\,x\ y\ \phi\ \psi\ \theta_R\ \theta_L\,]^T$ and τ_w is the torque vector of the wheel.

The motion equation of the robot with kinematics constraints is described as

$$M(q)\ddot{q} + C(q,\dot{q}) + G(q) = E\tau_w - A^T\lambda, \tag{13}$$

where $M(q) \in R^{6\times6}$ is the inertia matrix, $C(q,\dot{q}) \in R^{6\times1}$ is the Coriolis and centrifugal force vector, $G(q) \in R^{6\times1}$ is the force of gravity, A is the constraint matrix, $E \in R^{6\times2}$ is the input transformation matrix, $\tau_w \in R^{2\times1}$ is the input torque vector, and λ is the Lagrangian multiplier.

Solving Eq. (12) yields each term as follows:

$$M(q) = \begin{bmatrix} m_b & 0 & -m_b l_g s\phi_m s\psi_m & m_b l_g c\phi_m c\psi_m & 0 & 0 \\ 0 & m_b & m l_g c\phi_m s\psi_m & m_b l_g s\phi_m c\psi_m & 0 & 0 \\ -m_b l_g s\phi_m s\psi_m & m_b l_g c\phi_m s\psi_m & m_b l_g s^2\psi_m + I_{xx} s^2\psi_m + I_{zz} c^2\psi_m & 0 & 0 & 0 \\ m_b l_g c\phi_m c\psi_m & m_b l_g s\phi_m c\psi_m & 0 & m_b l_q^2 + I_{yy} & 0 & 0 \\ 0 & 0 & 0 & 0 & m_w r^2 & 0 \\ 0 & 0 & 0 & 0 & 0 & m_w r^2 \end{bmatrix},$$

$$C(q,\dot{q}) = \begin{bmatrix} -m_b l_g \sin\psi_m \cos\phi_m (\dot{\psi}_m^2 + \dot{\phi}_m^2) - 2 m_b l_g \dot{\psi}_m \dot{\phi}_m \cos\psi_m \sin\phi_m \\ -m_b l_g \sin\psi_m \sin\phi_m (\dot{\psi}_m^2 + \dot{\phi}_m^2) + 2 m_b l_g \dot{\psi}_m \dot{\phi}_m \cos\psi_m \cos\phi_m \\ 2(m_b l_g^2 + I_{xx} - I_{zz}) \sin\psi_m \cos\psi_m \dot{\psi}_m \dot{\phi}_m \\ -(m_b l_g + I_{xx} - I_{zz}) \sin\psi_m \cos\psi_m \dot{\phi}_m^2 \\ 0 \\ 0 \end{bmatrix}$$

$$C(q) = \begin{bmatrix} 0 \\ 0 \\ 0 \\ -m_b g l_g \sin\psi \\ 0 \\ 0 \end{bmatrix}, \quad E = \begin{bmatrix} 0 & 0 \\ 0 & 0 \\ 0 & 0 \\ -1 & -1 \\ 1 & 0 \\ 0 & 1 \end{bmatrix}, \quad \tau_w = \begin{bmatrix} \tau_{rw} \\ \tau_{lw} \end{bmatrix}.$$

The Lagrangian multiplier associated with kinematic constraint needs to be eliminated for simplicity. A new dynamic equation is derived by defining a new velocity vector ξ as $\xi = [v\dot{\phi}\dot{\psi}]^T$. Then the Jacobian relationship yields

$$\dot{q} = S(q)\xi, \tag{14}$$

where the vector $\dot{q} = [\dot{x}\dot{y}\dot{\phi}\dot{\psi}\dot{\theta}_R\dot{\theta}_L]^T$, and $S(q)$ is the necessary Jacobian matrix to eliminate the Lagrangian multiplier by satisfying the relationship $S^T A^T \lambda = 0$.

Then $S(q)$ is found to be

$$S(q) = \begin{bmatrix} \cos\varphi & 0 & 0 \\ \sin\varphi & 0 & 0 \\ 0 & 1 & 0 \\ 0 & 0 & 1 \\ \frac{1}{r} & \frac{L}{2r} & 0 \\ \frac{1}{r} & -\frac{L}{2r} & 0 \end{bmatrix}. \tag{15}$$

The constraint $A(q)$ matrix is given by kinematic constraint equations:

$$A(q) = \begin{bmatrix} \sin\varphi & -\cos\varphi & 0 & 0 & 0 & 0 \\ \cos\varphi & \sin\varphi & \frac{L}{2} & 0 & -r & 0 \\ \cos\varphi & \sin\varphi & -\frac{L}{2} & 0 & 0 & -r \end{bmatrix}. \tag{16}$$

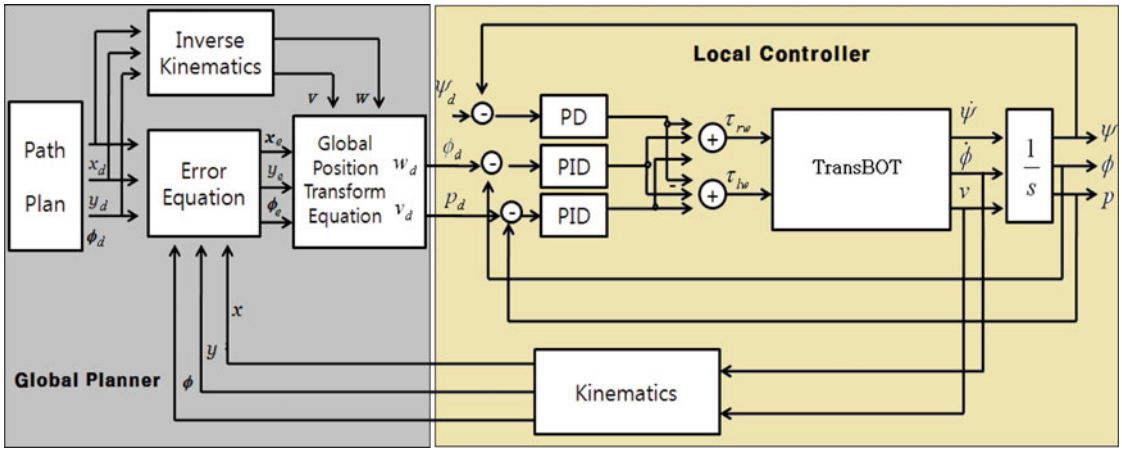

Fig. 2. (Colour online) Control structure.

Differentiating (14) yields the acceleration as

$$\ddot{q} = \dot{S}\xi + S\dot{\xi}. \tag{17}$$

Substituting (17) into (13) yields the dynamic equation as

$$M(q)S\dot{\xi} + M(q)\,\dot{S}\,\xi + C(q,\dot{q}) + G(q) = E\tau_w - A^T\lambda. \tag{18}$$

The multiplication of S^T on both sides to eliminate the Lagrangian multiplier yields

$$S^T M(q)S\dot{\xi} + S^T M(q)\,\dot{S}\,\xi + S^T(C(q,\dot{q}) + G(q)) = S^T E\tau_w. \tag{19}$$

A new dynamic equation is derived as

$$\bar{M}\dot{\xi} + \bar{C}\xi + \bar{G} = \bar{\tau}_w, \tag{20}$$

where $\bar{M} = S^T M(q)S \in R^{3\times3}$, $\bar{C} = S^T M(q)\,\dot{S} \in R^{3\times3}$, $\bar{G} = S^T(C(q,\dot{q}) + G(q)) \in R^{3\times1}$, and $\bar{\tau}_w = S^T E\tau_w \in R^{3\times1}$.

3. Control Schemes

3.1. Local control structure

Control of the vehicle can be obtained by designing appropriate torque for right and left wheels through linear controllers. Since the TransBOT is a combined system of inverted pendulum and mobile robot systems, control variables include a balancing angle ψ, an orientation angle ϕ, and a position p. Three separate linear controllers are used for the pendulum angle, the orientation angle, and the vehicle position. Proportional-derivative (PD) control, which is used for the balancing angle control, and proportional-integral-derivative (PID) control, which is used for the orientation and position control, are shown in Fig. 2. PD control is used for the balancing angle control to eliminate the effect of the accumulation error caused by a relative sensor.

The balancing angle error is defined as

$$e_\psi = \psi_d - \psi, \tag{21}$$

where ψ_d is the desired angle of the pendulum and ψ is the actual angle of the pendulum. For the balancing angle control, a PD controller is used:

$$u_\psi = k_{p\psi}e_\psi(t) + k_{d\psi}\,\dot{e}_\psi(t), \tag{22}$$

where $k_{p\psi}$ and $k_{d\psi}$ are the PD gains for the pendulum angle control.

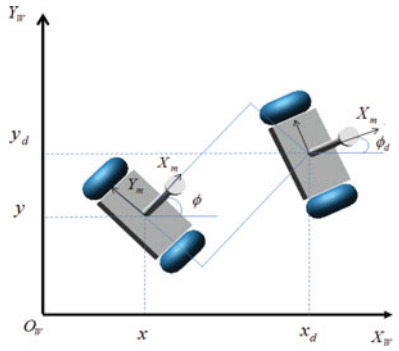

Fig. 3. (Colour online) Global trajectory tracking error coordinates.

The vehicle position error is defined as

$$e_p = p_d - p, \tag{23}$$

where $p_d(x_d, y_d)$ is the desired vehicle position and $p(x, y)$ is the actual position of the vehicle. For position control, the PID controller is given by

$$u_p = k_{pp}e_p(t) + k_{ip}\int e_p(t)dt + k_{dp}\dot{e}_p(t), \tag{24}$$

where k_{ip}, k_{dp}, k_{pp} are PID gains for the vehicle position control. The heading angle error is defined by

$$e_\phi = \phi_d - \phi, \tag{25}$$

where ϕ_d is the desired heading angle and ϕ is the actual angle of the vehicle. The PID controller output for the heading angle control is given by

$$u_\phi = k_{p\phi}e_\phi(t) + k_{i\phi}\int e_\phi(t)dt + k_{d\phi}\dot{e}_\phi(t), \tag{26}$$

where $k_{i\varphi}$, $k_{d\varphi}$, $k_{p\varphi}$ are the PID gains for heading angle control. The torque control input is the sum of three controller outputs,

$$\tau_{rw} = u_p + u_\phi + u_\psi, \tag{27}$$

$$\tau_{lw} = u_p - u_\phi + u_\psi, \tag{28}$$

where τ_{rw} is the torque input of right wheel and τ_{lw} is the torque input of left wheel. Figure 2 shows the overall control structure.

3.2. Global planner

The local controllers shown in Fig. 2 suffer from dead reckoning, which means that the vehicle totally relies on the encoder measurement for localization. However, when wheel slips occur in practice, the robot miscounts the encoder sensing data, resulting in a deviation error from the desired path. The vehicle does not know whether it is on the track. Global sensors, such as GPS, a beacon, or some other markers, can overcome the dead-reckoning problem.

To compensate for dead reckoning, the global planner was designed, as shown in Fig. 2, under the assumption that global sensors are available. The global positional error of the vehicle has been defined as $P_e^v = [\, x_e \;\; y_e \;\; e_\phi \,]^T$. Figure 3 shows the description of the global positional error coordinates.

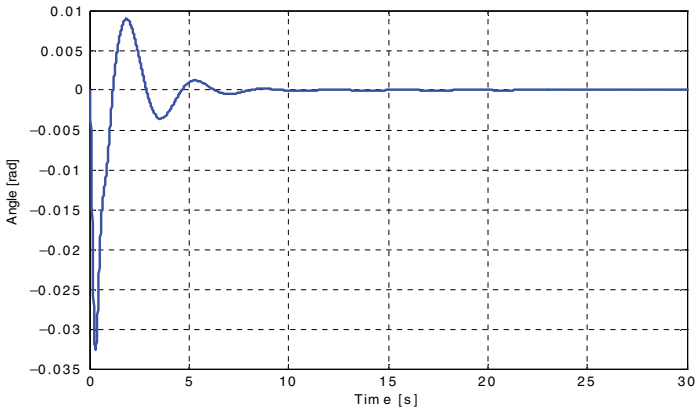

(a) Angle

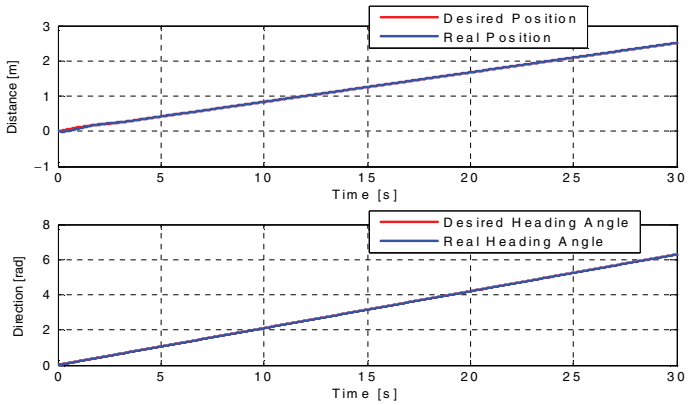

(b) Heading angle and position

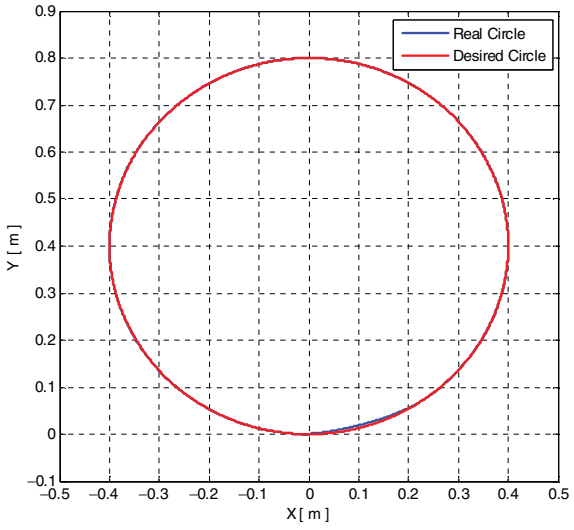

(c) Circular trajectory tracking

Fig. 4. (Colour online) Simulation results: (a) Angle; (b) heading angle and position, (c) circular trajectory tracking.

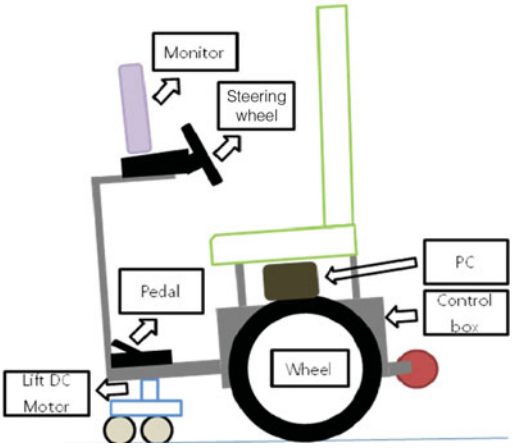

Fig. 5. (Colour online) Structure of TransBOT.

(a) Front view (b) Side view

Fig. 6. (Colour online) The actual TransBOT. (a) Front view, (b) side view.

The resulting positional error is described as

$$P_e^v = R_w^v(P_d^v - P_w^v) = \begin{bmatrix} \cos\varphi & \sin\varphi & 0 \\ -\sin\varphi & \cos\varphi & 0 \\ 0 & 0 & 1 \end{bmatrix} \left(P_d^v - P_w^v\right), \tag{29}$$

where R_w^v is the rotation matrix given in (1), P_d^v is the desired position of the vehicle $P_d^v = [x_d\, y_d \phi_d]^T$, and P_w^v is the vehicle position in global coordinates $P_w^v = [x y \phi]^T$.

The desired velocity profile can be obtained as[28]

$$\begin{bmatrix} v_d \\ w_d \end{bmatrix} = \begin{bmatrix} v\cos(\phi_e) + K_x x_e \\ w + v(K_y y_e + K_\phi \sin(\phi_e)) \end{bmatrix}, \tag{30}$$

where $x_e = \cos(\phi)(x_d - x) + \sin(\phi)(y_d - y)$, $y_e = -\sin(\phi)(x_d - x) + \cos(\phi)(y_d - y)$, $\phi_e = \phi_d - \phi$, and K_x, K_y, K_φ are gains. The desired velocity (30) was integrated to obtain the desired position from mobile robot kinematics.

3.3. Simulation

Simulations of the following circular trajectory was conducted based on the dynamics given in (20). The simulation models of the vehicle are $M(m_b + m_w) = 135$ kg, $r = 0.2$ m, $L = 0.7$ m, *and* $d = 0$. The simulation results are shown in Fig. 4. We see that the tracking performance was quite good. Other uncertain terms, such as slips and friction, were ignored in the simulation.

(a) The front casters with an electrical jack

(b) The back casters for protection

(c) The operator console

Fig. 7. (Colour online) The TransBOT. (a) The front casters with an electrical jack; (b) the back casters for protection; (c) the operator console.

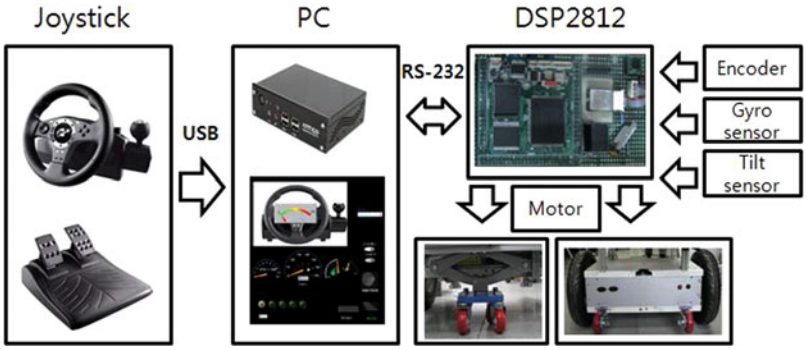

Fig. 8. (Colour online) Interface between parts in TransBOT.

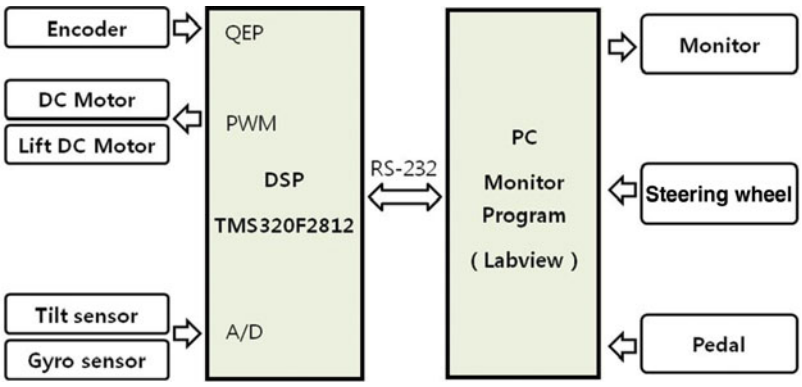

Fig. 9. (Colour online) Hardware Interface in TransBOT.

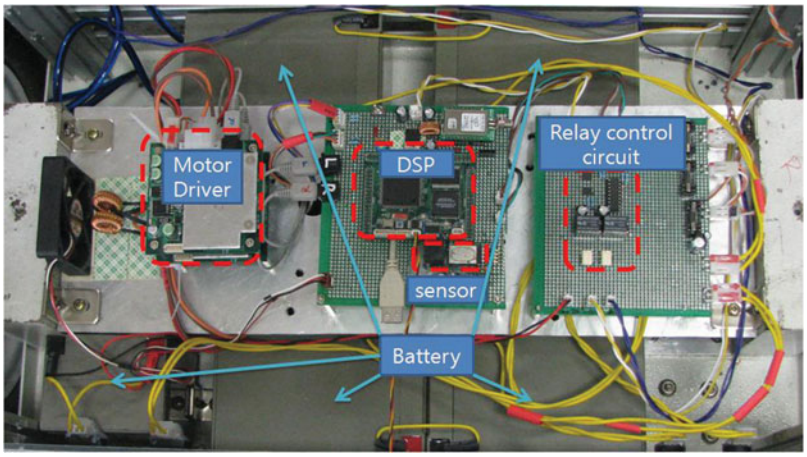

Fig. 10. (Colour online) The hardware structure of TransBOT.

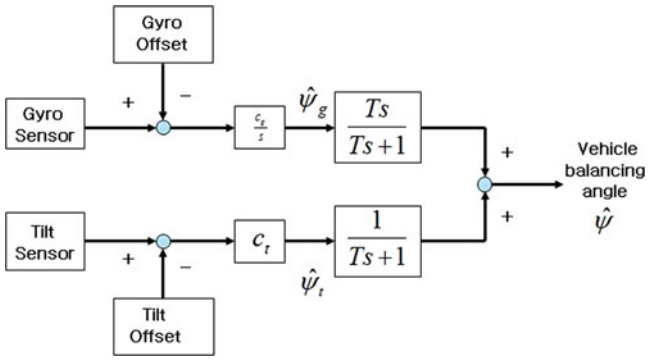

Fig. 11. (Colour online) The complementary sensor fusion block diagram.

4. TransBOT

4.1. Overall structure

The TransBOT comprises three major divisions: a driving segment, a handling segment, and a supporting segment. The schematic diagram of TransBOT is shown in Fig. 5. The driving segment contains two wheels, the control hardware, and a PC. The handling segment includes a steering wheel and a monitor, and the supporting segment has a pedal and a lifter.

Figure 6 shows a fully functional TransBOT. Two wheels are driven by two DC motors, and two sets of casters were mounted: one set was mounted on the front and the other was mounted on the back, as shown in Fig. 7. The front casters can easily stabilize the system by maintaining stable contact on the ground, while the back casters prevent the driver from falling. The graphic user interface (GUI) panel was designed to monitor the driving status. The driving mode can be chosen by selecting the position of casters in up or down position.

The TransBOT is controlled by a steering wheel and a pedal so that the desired position can be specified by pressing the pedal. A steering wheel can be rotated to control the direction. Initially, the TransBOT is in a four-wheel contact mode, and the driver can change the mode.

4.2. Hardware structure

The interface between mechanical and electrical parts is shown in Fig. 8. Input devices, such the steering wheel and pedal, interface with computer; the computer communicates with digital signal processor (DSP). As a main controller, the DSP deals with actuating the motors and the sensing interface.

A PC has interfaces with monitor, steering wheel, and pedal through the Labview program. DSP controller receives sensor data, processes filtering algorithms, calculates control algorithms, and

generates pulse width modulation (PWM) signals for motor drivers. The PC and DSP controller communicate with each other through an RS-232 communication channel, as shown in Fig. 9.

Figure 10 shows the actual layout of hardware. All of the hardware is located at the center of the wheel axis to obtain more accurate data. Batteries are evenly distributed to make a symmetrical structure. The motor drivers and the relay control circuits for the caster lifting motor were designed on a separate board, and were separately powered from the main control board of DSP and sensors. Insulation from actuators is required to minimize interference from actuators' noise.

5. Sensor Fusion

Two sensors are used to detect the balancing angle. These two sensors have different frequency responses. The gyro sensor measures the angular velocity and is designed for fast response. The tilt sensor measures the inclined angle and is designed for slow response. Thus, combining these two sensors may have the advantage of obtaining more accurate angle data.

Complementary filter is a combined filter of the low-pass filter $F_t(s)$ for the tilt sensor and the high-pass filter $F_g(s)$ for the gyro sensor,[17]

$$F_t(s) = \frac{1}{Ts+1}, \quad F_g(s) = \frac{Ts}{Ts+1}, \tag{31}$$

where T is the time constant. Since the sensor characteristics are different from sensors manufactured by the same company, the selection of T is found empirically.

Then each filtered output is added together to form a single value. Angle data can be obtained in all ranges of frequency,

$$F_t(s) + F_g(s) = 1. \tag{32}$$

Figure 11 shows the block diagram of a sensor fusion algorithm that obtained the balancing angle $\hat{\psi}$. The estimation of the balancing angle $\hat{\psi}$ can be obtained by filtering the real angle ψ as

$$\hat{\psi} = F_t(s)(\psi + \eta_H) + F_g(s)(\psi + \eta_L), \tag{33}$$

where η_H is high-frequency noise and η_L is low-frequency noise. The estimated angle becomes close to the real angle, since the noises are filtered, and are relatively small,

$$\hat{\psi} = \psi + F_t(s)\eta_H + F_g(s)\eta_L. \tag{34}$$

The offset value of each sensor is selected experimentally from the average values of sensor data. Gains C_t, C_s are used as a scale factor to normalize the data.

6. Experimental Studies

6.1. Balancing control test

The first experiment is to control TransBOT without a driver. Initially, the unmanned TransBOT was tested for balancing, navigation, and control. The TransBOT is controlled remotely by an operator through wireless communication. Figure 12 shows plots of the balancing angle, the position, and the orientation angle. To create disturbance, this study hit the vehicle at roughly 30- and 40-s markers while the vehicle was balancing, as in Fig. 12(a). The plot shows that the TransBOT performs well enough to maintain balance under an intentional disturbance. Figure 12(b) shows the corresponding position data while the vehicle was balancing.

6.2. Remote control

We remotely controlled the vehicle with a 25-kg payload with a joystick. The balancing and orientation angles are controlled and plotted in Figs. 13(a) and 13(b) respectively. It is important to note that the balancing angle settled at roughly 0.04 rad. This behavior occurred because the vehicle is not

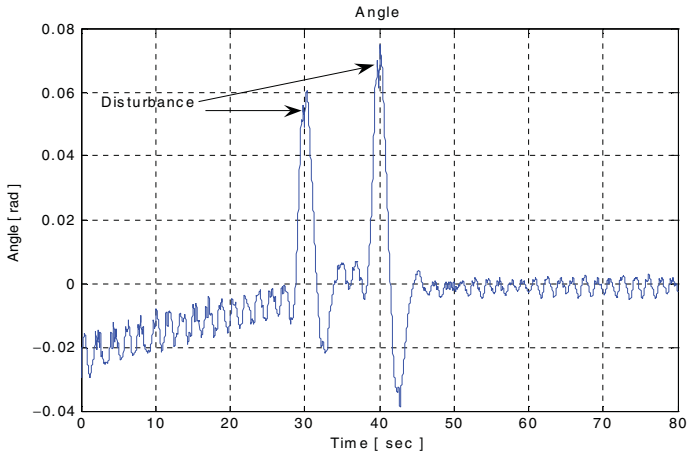

(a) Balancing angle control

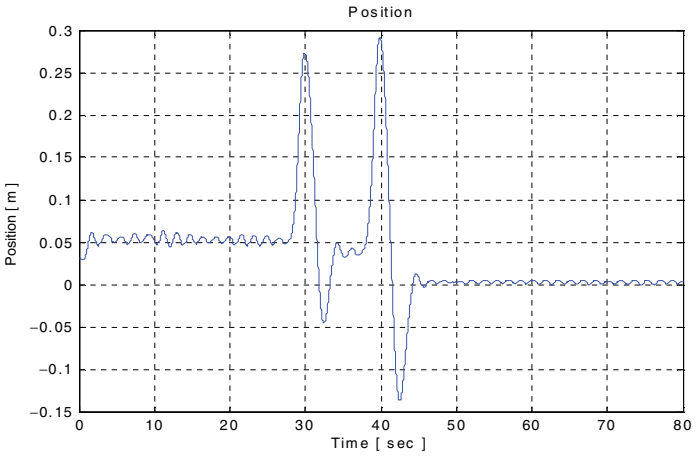

(b) Position control

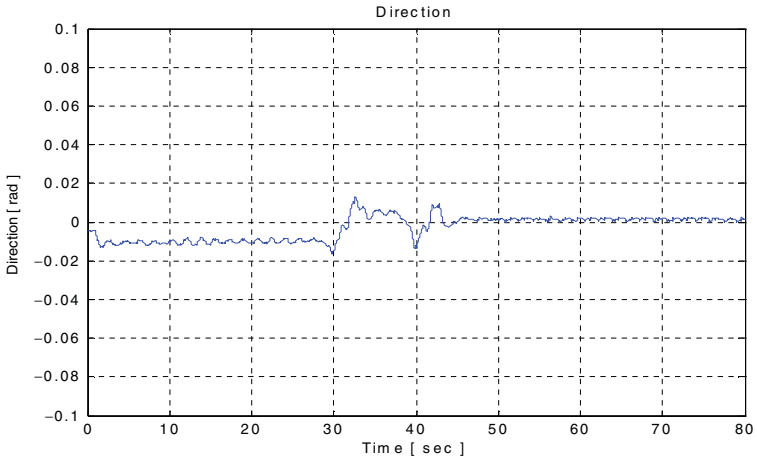

(c) Orientation angle control

Fig. 12. (Colour online) Test of unmanned control: (a) Balancing angle control, (b) position control, (c) orientation angle control.

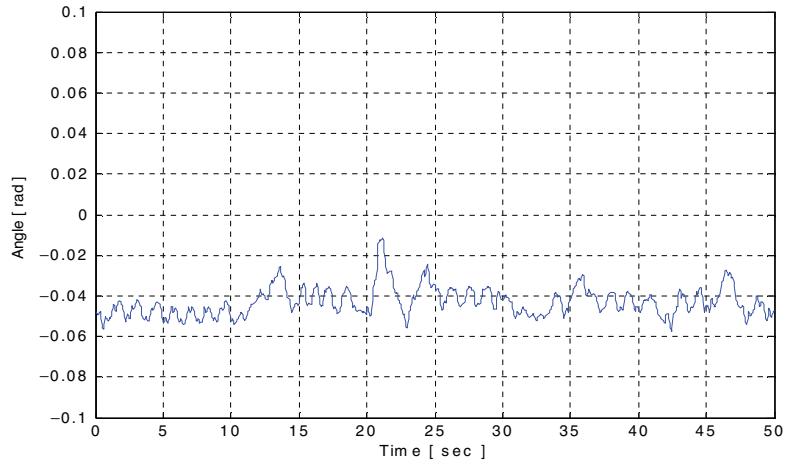

(a) Balancing angle

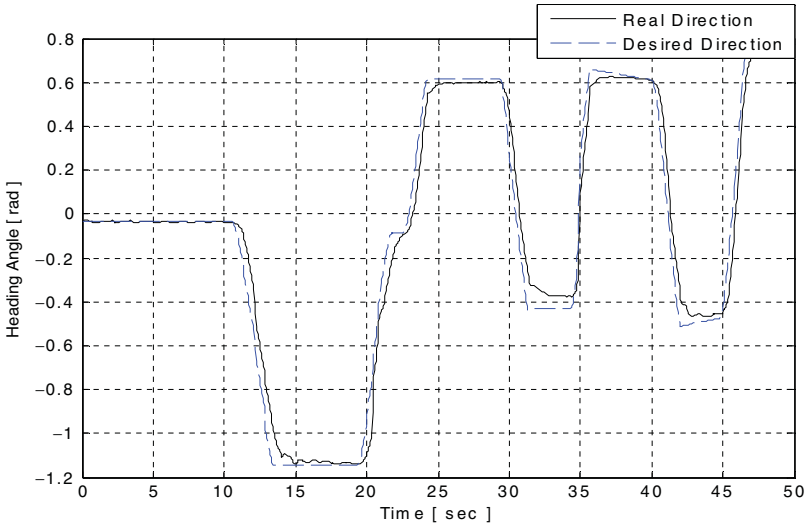

(b) Orientation angle

Fig. 13. (Colour online) The test of joystick control: (a) Balancing angle, (b) orientation angle.

perfectly symmetrical. This implies that different desired balancing angle values should be specified for stable balancing with respect to different payloads.

6.3. Balancing tests for different drivers

Each driver who tested the TransBOT had different weight. Since the payload was changing, the corresponding controller gains were required to be changed for stable balancing performance. Table II lists desired angle values for different weight ranges, and controller gains for balancing control and position control.

These values are found empirically through several experiments. Here the controller gains for the heading angle are fixed without modifications.

Initially, the TransBOT was stabilized by making the following three contact points with the front ball caster. Then the driver changed from the driving mode to the balancing mode by lifting the front caster.

1. Weights of 43 kg: A person weighing 43 kg drove the TransBOT. Figure 14 shows the results of driving test. The person moved forward by about 0.5 m and came back while balancing.

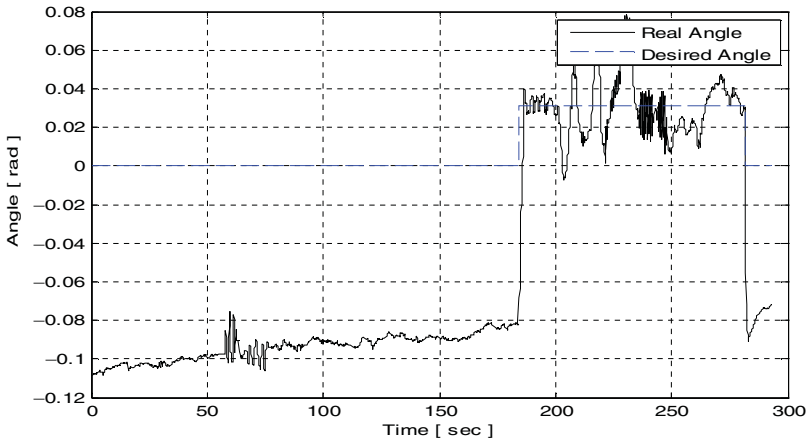

(a) Balancing angle

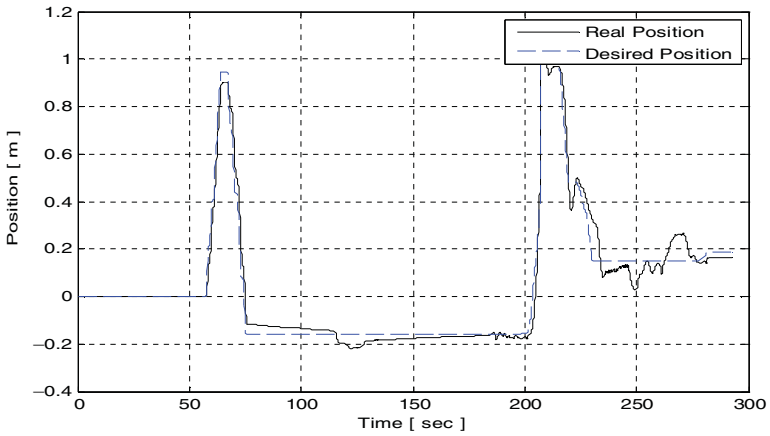

(b) Position

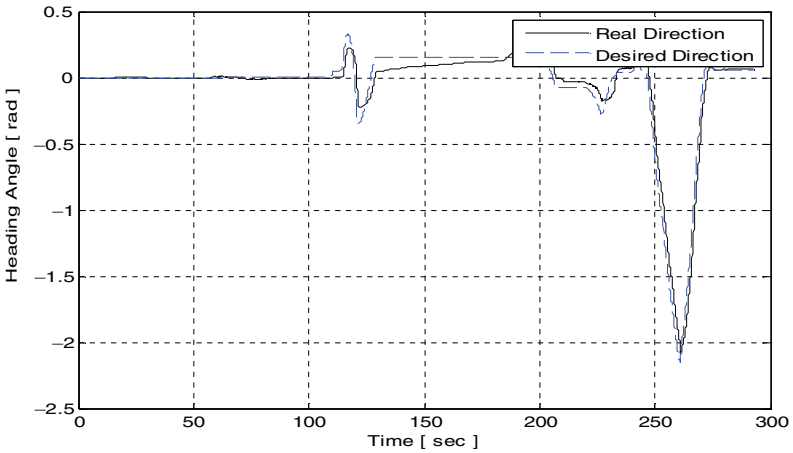

(c) Heading angle

Fig. 14. (Colour online) The balancing test results for 43 kg: (a) Balancing angle, (b) position, (c) heading angle.

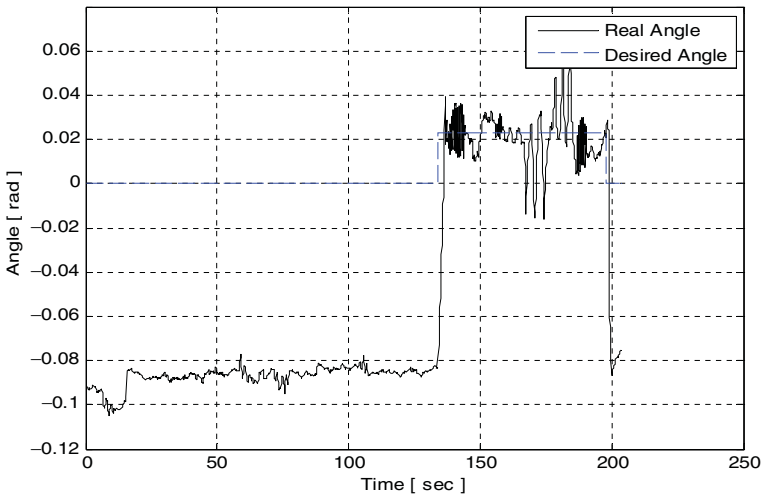

(a) Balancing angle

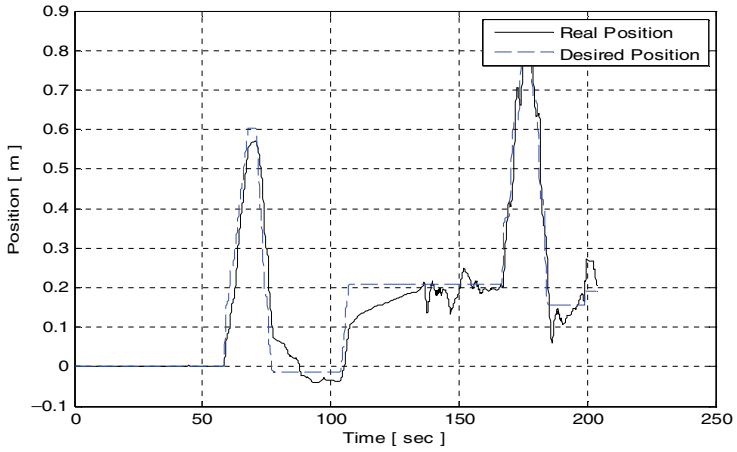

(b) Position

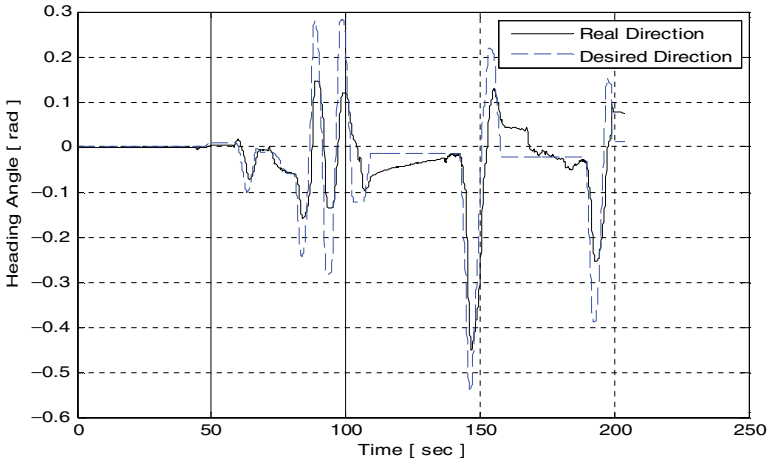

(c) Heading angle

Fig. 15. (Colour online) The balancing test results for 55 kg: (a) Balancing angle, (b) position, (c) heading angle.

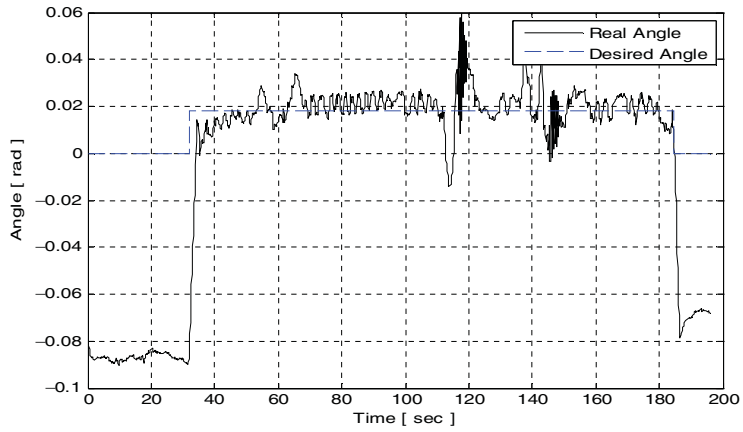

(a) Balancing angle

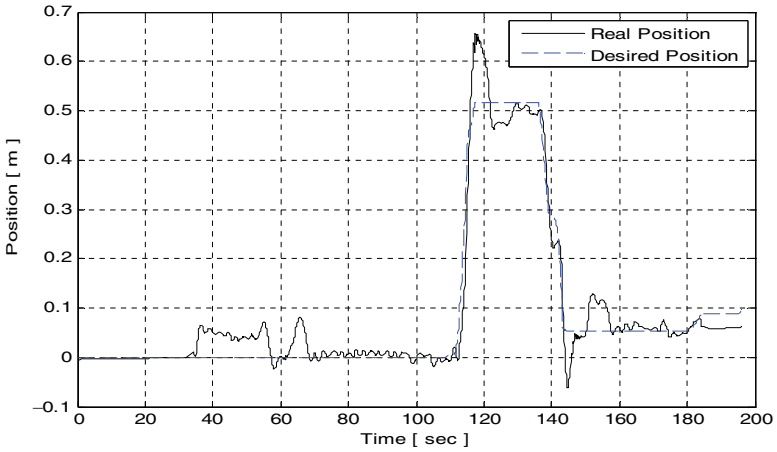

(b) Position

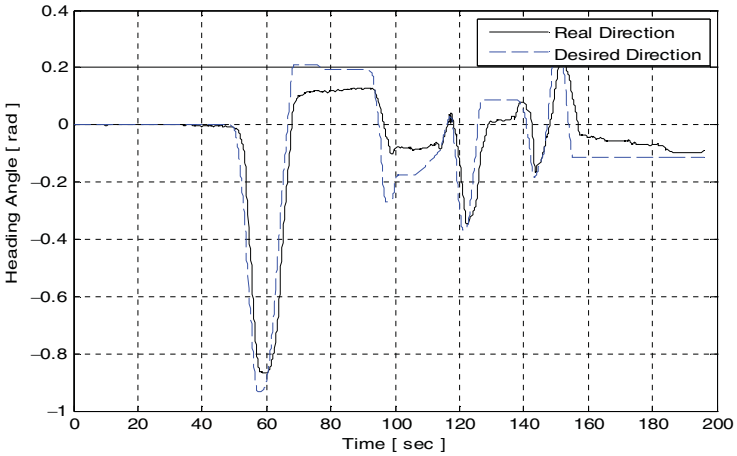

(c) Heading angle

Fig. 16. (Colour online) The balancing test results for 62 kg: (a) Balancing angle, (b) position, (c) heading angle.

Table II. The desired angle with respect to different weights.

		PD gains for balancing angle		PID gains for position		
Weight range (kg)	Desired angle (rad)	$k_{p\psi}$	$k_{d\psi}$	k_{pp}	k_{ip}	k_{dp}
40–49	0.0314	190	12	−15	−12	−1
50–59	0.023	195	12	−15	−14	−1
60–69	0.019	200	14	−17	−13	−1
70–79	0.01	205	14	−18	−14	−1

Fig. 17. (Colour online) Indoor driving experiment: balancing mode.

Figure 14(a) shows the balancing angle, indicating good balance. The desired balancing angle was set to 0.0314 rad, as listed in Table II. The corresponding position and heading angle movements are shown in Figs. 14(b) and (c) respectively.

2. Weights of 55 kg: The same experiment was conducted for 55-kg weight. The desired balancing angle was set to 0.023 rad as shown in Fig. 15.
3. Weights of 62 kg: A person who weighs 62 kg drove the TransBOT forward by about 0.5 m and came back while balancing. The desired balancing angle was set to 0.019 rad. Figure 16(a) shows that the balancing angle is maintained at around 0.019 rad. The corresponding position and heading angle movements are shown in Figs. 16(b) and (c) respectively.

We saw small oscillations with a maximum of about 0.06 rad, which is 3.4° in the balancing angle plots. However, these angles have minimal effects on drivers.

6.4. Indoor driving test

Figure 17 shows the indoor driving test. The driver began driving the TransBOT in driving mode, which occurs when the unit has three or four point contacts on the ground. Then the driver switched from the driving mode to the balancing mode by lifting the front caster. Using the balancing mode, the driver made several turns in a narrow space and then proceeded to navigate around the floor of the shown building.

The driver went into an elevator to head outside. Figure 18 shows the corresponding plots of Fig. 17. Figure 19 shows the driving test of going inside an elevator. One advantage of the balancing mode of the TransBOT is the ability of making turns inside an elevator.

6.5. Outdoor driving test

The next driving test was performed outdoors. Figure 20 shows the video-cut images of outdoor driving test. Even with the ground not being flat, the TransBOT maintained a good balancing performance.

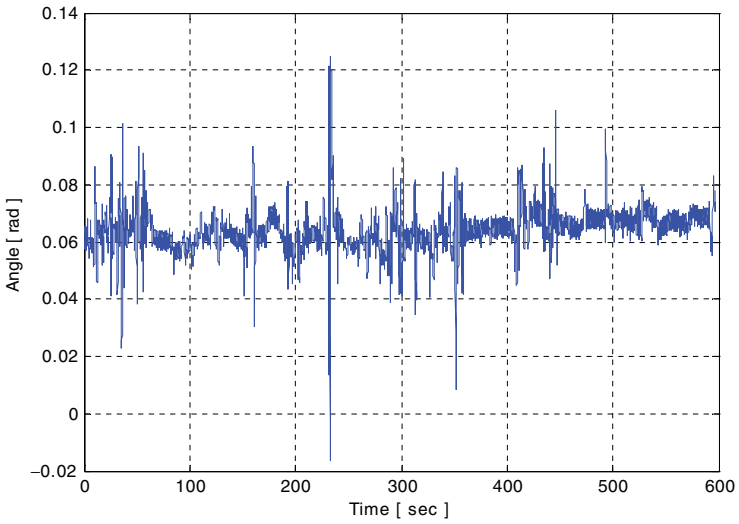

(a) Balancing angle

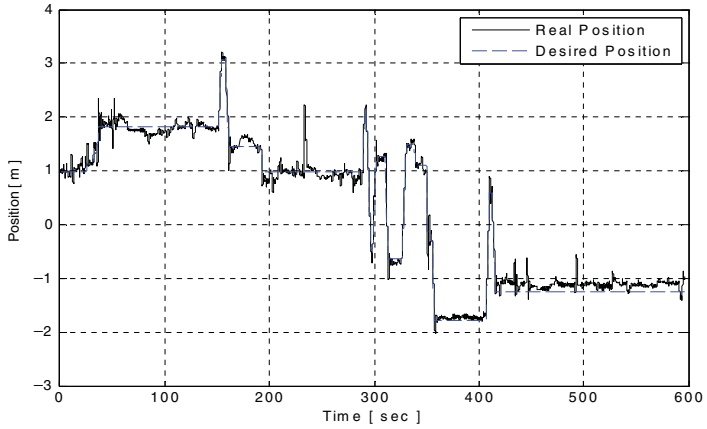

(b) Position

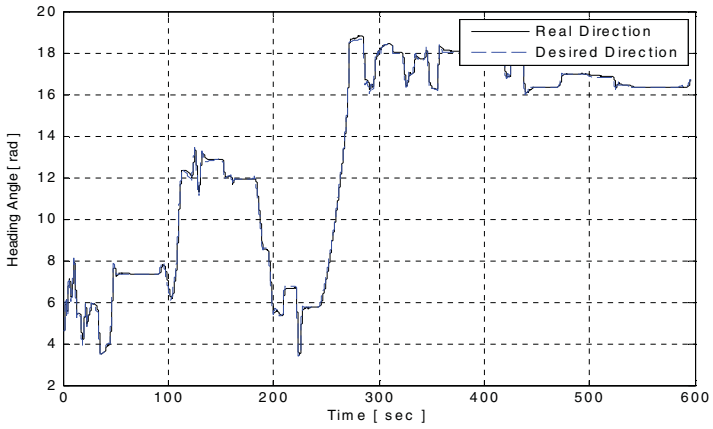

(c) Heading angle

Fig. 18. (Colour online) Indoor driving results: balancing mode. (a) Balancing angle, (b) position, (c) heading angle.

Fig. 19. (Colour online) Going into elevator.

Fig. 20. (Colour online) The outdoor driving experiment.

Figure 21 shows the plots of driving test in the outdoor environment. The balancing angle shown in Fig. 21(a) demonstrated that switching from the balancing mode to the driving mode had a stable transition. The plot shows a good balancing performance while driving in the balancing mode. When in the driving mode, we observed a disturbance effect from road conditions, as marked with red circles in Fig. 21(a). After switching to the driving mode, the balancing angle became -0.1 rad. This means that the front caster contacted the ground, creating a stable posture. The corresponding position and orientation plots are shown in Figs. 21(b) and (c) respectively.

7. Conclusions

The concept of the inverted pendulum system was applied to a two-wheel balancing vehicle robot as a feasible future vehicle for carrying a human passenger. The balancing mechanism of TransBOT maintained both desired angle and position simultaneously for effective driving in an urban area. Performing the driving tests of TransBOT in indoor and outdoor environments proved the feasibility of TransBOT as a transportation vehicle.

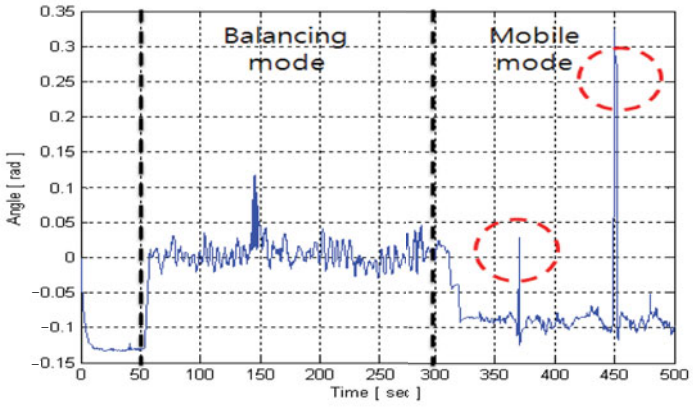

(a) Balancing angle

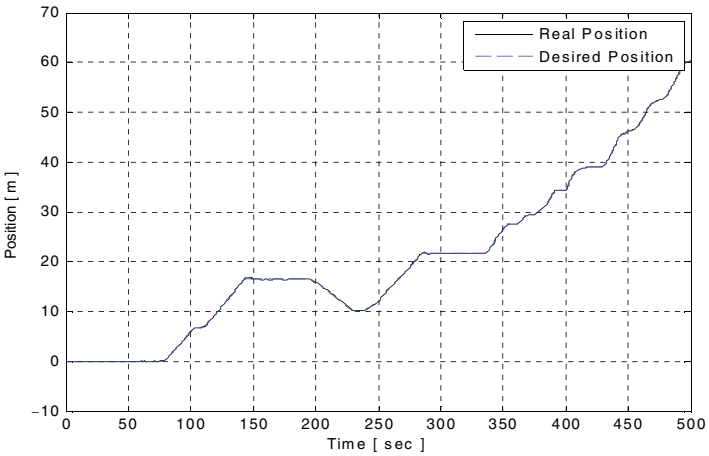

(b) Position control

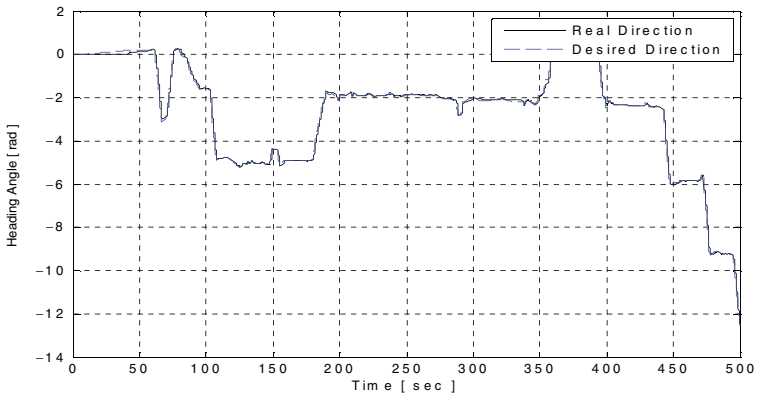

(c) Orientation angle control

Fig. 21. (Colour online) The outdoor navigation results: (a) Balancing angle, (b) position control, (c) orientation angle control.

The experimental results for different passengers confirmed that the gain scheduling method along with specifying the desired balancing angle with respect to different weights was efficiently used for stable balancing performance. Thus, either robust control algorithms or intelligent control methods are required to deal with uncertainties such as different weights or rough road conditions.

Here we proved only the feasibility of using TransBOT as a future personal vehicle. However, to be in the market, there are still many problems to be solved. First, the reliability of riding needs is to be guaranteed. The comfort and stability of passengers of all age groups need to be satisfied. Lastly, a familiar body design is also required.

Acknowledgements
This work was supported in part by the 2012 Basic Research Program (NRF-2010-0024904) through Korea Research Foundation and the Center for Autonomous Intelligent Manipulation (AIM) for service robots of the Ministry of Knowledge Economy (MKE) under the Human Resources Development Program for Convergence Robot Specialists Support Program supervised by the National IT Industry Promotion Agency (NIPA) under NIPA-2012-H1502-12-1002.

References

1. "Segway." (2014) Available at: http://www.segway.com (online).
2. F. Grasser, A. Darrigo, S. Colombi and A. Rufer, "JOE: A mobile, inverted pendulum," *IEEE Trans. Ind. Electron.* **49**(1), 107–114 (2002).
3. K. Pathak, J. Franch and S. Agrawal, "Velocity and position control of a wheeled inverted pendulum by partial feedback linearization," *IEEE Trans. Robot.* **21**, 505–513 (2005).
4. S. S. Kim and S. Jung, "Control experiment of a wheel-driven mobile inverted pendulum using neural network," *IEEE Trans. Control Syst. Technol.* **16**(2), 297–303 (2008).
5. C. H. Huang, W. J. Wang and C. H. Chiu, "Design and implementation of fuzzy control on a two-wheel inverted pendulum system," *IEEE Trans. Ind. Electron.* **58**(7), 2988–3001 (2011).
6. C. C. Tsai, H. C. Huang and S. C. Lin, "Adaptive neural network control of self-balancing two-wheeled scooter," *IEEE Trans. Ind. Electron.* **57**(4), 1420–1428 (2010).
7. H., Tirmant, M. Baloh, L. Vermeiren, T. M. Guerra and M. Parent, "B2, An Alternative Two-Wheeled Vehicle for an Automated Urban Transportation System," *Proceedings of the IEEE Intelligent Vehicle Symposium*, Versailles, France (Jun. 17–21, 2002) pp. 594–603.
8. P. K. Abeygunawardhana and T. Murakami, "Vibration suppression of two-wheel mobile manipulator using resonance-ratio-control-based null-space control," *IEEE Trans. Ind. Electron.* **57**(12), 4137–4145 (2010).
9. S. H. Jeong and T. Takahashi, "Wheeled Inverted Pendulum Type Assistant Robot: Inverted Mobile, and Sitting Motion," *IEEE/RSJ International Conference on Intelligent Robots and Systems*, San Diego, USA (Oct. 29–Nov. 2, 2007) pp. 1932–1937.
10. R. O. Ambrose, R. T. Savely, S. M Goza, P. Strawser, M. A. Diftler, I. Spain and N. Radford, "Mobile Manipulation Using NASA's Robonaut," *IEEE Conference on Robotics and Automations*, New Orleans, USA (Apr. 26–May 1, 2004) pp. 2104–2109.
11. H. J. Lee, H. J. Choi, J. H. Park, J. H. Lee and S. Jung, "Center of Gravity-Based Control of a Humanoid Balancing Robot for Boxing Games: BalBOT V," *International Conference on Control, Automation and Systems (ICCAS) - The Society of Instrument and Control Engineers (SICE)* (2009) pp. 124–128.
12. K. Teeyapan, J. Wang, T. Kunz and M. Stilman, "Robot Limbo: Optimized Planning and Control for Dynamically Stable Robots Under Vertical Obstacles," *Proceedings of the IEEE Conference on Robotics and Automations*, Anchorage, Alaska (May 3–8, 2010) pp. 4519–4524.
13. K. Sasaki and T. Murakami, "Pushing Operation by Two-Wheel Inverted Mobile Manipulator," *IEEE Workshop on Advanced Motion Control*, Trento, Italy (Mar. 26–28, 2008) pp. 33–37.
14. P. K. Abeygunawardhana and M. Toshiyuki, "Environmental Interaction of Two Wheeled Mobile Manipulator by Using Reaction Torque Observer," *IEEE Workshop on Advanced Motion Control*, Trento, Italy (Mar. 26–28, 2008) pp. 348–353.
15. S. J. Lee and S. Jung, "Stabilization of a Two Wheeled Mobile Robot System Under External Force," *Proceedings of International Conference on Ubiquitous Robots and Ambient Antelligence (URAI)*, Busan, Korea (Nov. 24–27, 2010), pp. 225–228.
16. R. Imamura, T. Takei and S. Yuta, "Sensor Drift Compensation and Control of a Wheeled Inverted Pendulum Mobile Robot," *IEEE Workshop on Advanced Motion Control*, Trento, Italy (Mar. 26–28, 2008) pp. 137–142.
17. H. G. Lee and S. Jung, "Gyro Sensor Drift Compensation by Kalman Filter to Control a Mobile Inverted Pendulum Robot System," *Proceedings of the IEEE Conference on Industrial Technology*, Churchill, Australia (Feb. 10–13, 2009) pp. 1026–1031.
18. G. H. Lee, S. J. Lee and S. Jung, "Line Tracking Control Using Visual Feedback of a Mobile Inverted Pendulum: BalBOT IV," *Proceedings of the 14th IASTED International Conference on Robotics and Automation*, Cambridge, USA (Nov. 4–6, 2009) pp. 188–193.
19. J. Angeles, "An innovative drive for two-wheeled mobile robot," *IEEE/ASME Trans. Mechatronics* **10**(1), 43–48 (2005).
20. Y. S. Xu and K. W. Au, "Stabilization and path following of a single wheel robot," *IEEE/ASME Trans. Mechatronics* **9**(2), 407–419 (2004).

21. H. J. Jin, J. M. Hwang and J. M. Lee, "A balancing control strategy for a one-wheel pendulum robot based on dynamic model decomposition: Simulation and experiments," *IEEE/ASME Trans. Mechatronics* **16**(4), 763–768 (2011).
22. P. Oryschuk, A. Salerrno, A. M. Al-Husseini and J. Angeles, "Experimental validation of an underactuated two-wheeled robot," *IEEE/ASME Trans. Mechatronics* **14**(2), 252–257 (2009).
23. J. Baber, L. T. Noel and M. Parent, "Personal rapid transportation," *Computing & Control Engineering Journal* **14**(4), 20–21 (2003).
24. T. Ishii, M. Iguchi, T. Nakahara, Y. Kohsaka and Y. Doi, "Computer-controlled mini car system in Expo'70: An experiment in a new personal urban transportation system," *IEEE Trans. Veh. Technol.* **21**(3), 77–91 (1972).
25. C. B. Low and D. Wang, "GPS-based tracking control for a car-like wheeled mobile robots with skidding and slipping," *IEEE/ASME Trans. Mechatronics* **13**(4), 480–484 (2008).
26. K. Hirata, M. Kamatani and T. Murakami, "Advanced Motion Control of Two-Wheel Wheelchair for Slope Environment," *Proceedings of International Conference on Industrial Electronics, Control and Instrumentation (IECON)*, Vienna, Austria (Nov. 10–13, 2013) pp. 6436–6441.
27. H. J. Lee, H. W. Kim and S. Jung, "Development of a Mobile Inverted Pendulum Robot System as a Personal Transportation Vehicle with Two Driving Modes: TransBOT," *Proceedings of the World Automation Congress (WAC)*, Kobe, Japan (Sep. 19–23, 2010) pp. 1–5.
28. Y. Kanayama, Y. Kimura, F. Miyazaki and T. Noguchi, "A Stable Tracking Control Method for an Autonomous Mobile Robot," *Proceedings of the IEEE International Conference on Robotics and Automation*, Cinoinnati, USA (May 13–18, 1990) pp. 384–389.